atmosphere

MDPI

Article

The Spatiotemporal Distribution of Air Pollutants and Their Relationship with Land-Use Patterns in Hangzhou City, China

Sheng Zheng [1,*], Xueyuan Zhou [1], Ramesh P. Singh [2,*], Yuzhe Wu [1], Yanmei Ye [1] and Cifang Wu [1]

[1] Department of Land Management, Zhejiang University, Hangzhou 310058, China; zhouxyzju@163.com (X.Z.); wuyuzhe@zju.edu.cn (Y.W.); yeyanmei@zju.edu.cn (Y.Y.); wucifang@zju.edu.cn (C.W.)

[2] School of Life and Environmental Sciences, Schmid College of Science and Technology, Chapman University, One University Drive, Orange, CA 92866, USA

* Correspondence: shengzheng@zju.edu.cn (S.Z.); rsingh@chapman.edu (R.P.S.)

Received: 26 April 2017; Accepted: 16 June 2017; Published: 20 June 2017

Abstract: Air pollution contributes to a large fraction of the total mortality estimated under the global burden of disease project (GBD) of the World Health Organization (WHO). This paper discusses an integrated study to obtain the spatiotemporal characteristics of particulate matter (PM_{10} and $PM_{2.5}$) and trace gases (O_3, SO_2, NO_2, and CO) pollutants in Hangzhou City (China) for the years 2014–2016. Our detailed analysis shows a relationship between air pollutants and land-use/land-cover change. Air quality parameters ($PM_{2.5}$ and PM_{10}) and trace gases (SO_2, NO_2, and CO) show strong monthly variations in the months of January (higher values) and July (lower values). During monsoon and summer seasons, air quality and trace gases show low values, whereas ozone (O_3) is higher in the summer and lower in the winter. The spatial distribution of air pollutants is retrieved using the kriging method at the monitoring sites in Hangzhou City. We have considered normalized difference vegetation index (NDVI) and land surface temperature (LST) from the Landsat 8 data. The correlation between air pollutants and land use at the street-town unit suggests that areas with low NDVI, high road density, large built-up density, and LST are consistent with high concentrations of particulate matter and SO_2, NO_2, and CO. Among the trace gases, NO_2 is found to be the most sensitive element affected by land use patterns, and O_3 shows weak correlation with land use. SO_2 shows a strong positive correlation with road density and LST, whereas CO shows positive correlation with the built-up density, LST, and population density.

Keywords: trace gases; particulate matter; land use; Hangzhou (China)

1. Introduction

Air pollution in general in Asia, especially in China and India has increased since the Industrial Revolution, i.e., during the Anthropocene epoch [1,2]. The Global Burden of Disease (GBD) study was first published by the World Health Organization (WHO) in 1990 and the report is updated every 10 years. According to the GBD study of 2010, outdoor air pollution, especially fine particles, is a serious health risk [3]. Among the 20 leading risk factor causes of death in 2010 globally, outdoor air pollution ranked ninth in the world and fourth in China. Outdoor pollution in the form of fine particles causes 3.2 million premature deaths globally, and 1.2 million premature deaths occurred in China in 2010. Outdoor air pollution is considered as slow poison, affecting health slowly so that people suffer for a long period, and also affecting day-to-day weather conditions. During the winter, air pollutants (concentrations of air particulate matter and trace gases) play an important role in the formation of dense fog and haze [4–8], affecting the daily lives of people in Hangzhou and the surrounding regions.

Land-use/land-cover (LULC) are important factors in global environment and climate change. Land use has rapidly changed in Asian countries in general, in particular in China. Land-use change has dramatically altered the Earth's landscape, chemical fluxes, and radiation budget. The rapid land-use change is due to the population growth, which is related to the urban sprawl, farmland displacement, and deforestation, leading to a loss of arable land and habitat destruction. These losses have also contributed to growing atmospheric pollution at the local, regional, and global scales. Changes in land cover, responding to both human forcing and natural factors, play a key role in modulating air quality and changing climate [9]. Land-use change contributes to the change in the composition of gases in the atmosphere, as well as changes in atmospheric chemical properties and processes, resulting in pronounced changes in the concentrations of greenhouse gases including carbon dioxide and methane [6,10]. An analysis of the carbon dioxide flux, releasing to or removed from the atmosphere, results from land-use change and is related to the amounts of organic carbon within an ecosystem associated with the changes in forest cover. There has been a net release of carbon from terrestrial ecosystems worldwide since 1860, and the annual release was greater compared to the release of carbon from fossil fuels in the past 150 years [11]. There is clear evidence from the analysis of gases trapped in dated cores due to industrial and agricultural production activities, and atmospheric methane concentrations have more than doubled in the last 200 years [12,13]. The major methane sources include enteric fermentation of carbohydrates by ruminants, anaerobic decomposition of organic material in natural wetlands, landfills, and rice paddies. The amount of methane released from wetlands accounts for 20% of the total amount of methane in the atmosphere. Meanwhile, methane can be oxidized to carbon monoxide. Model-based estimates show 60% of carbon monoxide attributes to land-use change [14]. Taha [15] analyzed the effects of increased urban vegetation on the ozone and found that the net effect of increased urban vegetation shows decrease in ozone concentrations if the additional vegetation is low emitters. Tree species release appreciable quantities of hydrocarbons to the atmosphere, thus contributing to air pollution. Urban air quality is related to nitrogen oxides (NO_2), carbon monoxide (CO), sulfur dioxide (SO_2), ozone (O_3), and carbon dioxide (CO_2) as well as the anthropogenic and biogenic particulate matter ($PM_{2.5}$, PM_{10}). Urban land-use change has a significant impact on the concentrations of these atmospheric pollutants. Peng et al. [16] analyzed the relationship between land-use change and its urban air environmental impacts, and found an impact of land use on urban air quality. The NO_2 change results from woodland are obvious, and the impact on the highest concentration of total suspended particulate matter from the urban land use is pronounced. By applying the land-use regression model, outdoor air pollution (NO_2, $PM_{2.5}$) based on land-use parameters was estimated at a high spatial resolution [17–21]. The satellite aerosol data, in conjunction with comprehensive meteorological and geographical data, are used to improve the estimation of $PM_{2.5}$ concentration [22]. In addition, the layout of an urban area can impact air pollution via changes in emission and their spatial distribution based on cross-sectional observations for 111 U.S. urban areas. Aspects of urban form evaluated include city shape, road density, population density, and the jobs–housing imbalance [23]. Bechle et al. [24] have investigated the relationship between satellite-derived NO_2 and 83 urban city areas globally, and found that urban cities with highly contiguous built-up areas have, on average, lower NO_2 concentrations; more populous cities tend to exhibit poor air quality. Earlier studies mainly focus on the qualitative impact of land-use change on limited atmospheric pollutants without giving details of the physical process.

The Yangtze River Delta (YRD) region has experienced a rapid urbanization process accompanied by economic development during the last few decades. The conversion of vegetated and irrigated cropland into an urban area significantly changes the temperature and wind speed [25]. The YRD and surrounding areas are affected by the dense haze [26,27]. Hangzhou is one of the central cities in the YRD economic circle, and due to the major and rapid land-use change, environmental quality has changed rapidly in the last 30 years. Efforts have been made to study the air quality in Hangzhou, China [7,28–32]. Local vehicle emissions in Hangzhou City were considered a major contributor to $PM_{2.5}$ pollution, and local emissions rather than regional transport were the major source contributing to pollution

episodes [32]. Eliminating substandard vehicles, upgrading vehicle standards, supplying low-sulfur oil, and introducing alternative fuel vehicles could simultaneously reduce the four key pollutants (CO, volatile organic compounds, nitrogen oxides, and particulate matter) [28]. The impact of urbanization on air pollution diffusion in Hangzhou City has been investigated. The present results show that the changes in the meteorological environment decreased the urban atmosphere's diffusion capability, and therefore increased urban pollutant concentrations [30]. However, few quantitative studies of the relationship between land use and air quality have been carried out in Hangzhou, China. In the present study, the spatiotemporal characteristics of air pollution in the Hangzhou area are discussed for the years 2014–2016. We mainly focus on the characteristics of trace gases (SO_2, NO_2, CO, O_3) and particulate matter ($PM_{2.5}$ and PM_{10}). The relationship between air pollutants and land-use change including vegetation, land surface temperature, and urban settings is analyzed for Hangzhou City.

2. Study Area

Hangzhou City is the capital and most populous city of Zhejiang Province in East China. It is located in northwestern Zhejiang province, in the south-central portion of the Yangtze River Delta. It covers an area of 16,596 km^2, with population density of 536 persons/km^2 (as of 2014). Hangzhou experiences a humid subtropical climate with four distinctive seasons, characterized by long, hot humid summers and chilly, cloudy winters. The average annual precipitation is 1438 mm, abundant during the summer and relatively low during the winter. In late summer, Hangzhou suffers from typhoon storms. The prevailing wind direction is mainly southerly during the summer and northerly during the winter. The atmospheric structure is relatively stable, and temperature inversion often occurs in late autumn and winter. Hangzhou City comprises nine municipal districts. Among the nine districts, six central urban districts (Shangcheng, Xiacheng, Jianggan, Gongshu, Xihu, and Binjiang) cover an area of 683 km^2 with a population of 3.6 million for the year 2013 [33,34].

There are 11 state-controlled air pollution monitoring sites located in Hangzhou City. For the present study, we have considered monitoring sites in and near the urban central urban districts to study the impact of urban land-use/land-cover change. The location of Hangzhou in China and the spatial distribution of the 10 state-controlled monitoring sites in the eight districts of Hangzhou are shown in Figure 1a,b. The names of the monitoring sites corresponding to the site numbers in Figure 1b are listed in Table 1. Figure 1c shows the street-town boundary, West Lake (a tourist spot), and the center of the urban area. Street towns, also called sub-districts, are the smallest geographic unit at which census data are released to the public [35]. It is also the spatial unit where many municipal policies are made and implemented. The urban core area is designated as the downtown area including street-towns of Qingbo, Hubin, Xiaoying, Wulin, Tianshui, Changqing, and Chaoming, and it is surrounded by the city ring road, which includes the main central business district.

Table 1. List of monitoring sites in Hangzhou, China.

Sites	Name of Site	Sites	Name of Site
Site 1	Linpinzhen	**Site 6**	Zhejiangnongda
Site 2	Xiasha	**Site 7**	Wolongqiao
Site 3	Hemuxiaoxue	**Site 8**	Binjiang
Site 4	Chaohuiwuqu	**Site 9**	Chengxiangzhen
Site 5	Xixi	**Site 10**	Yunqi

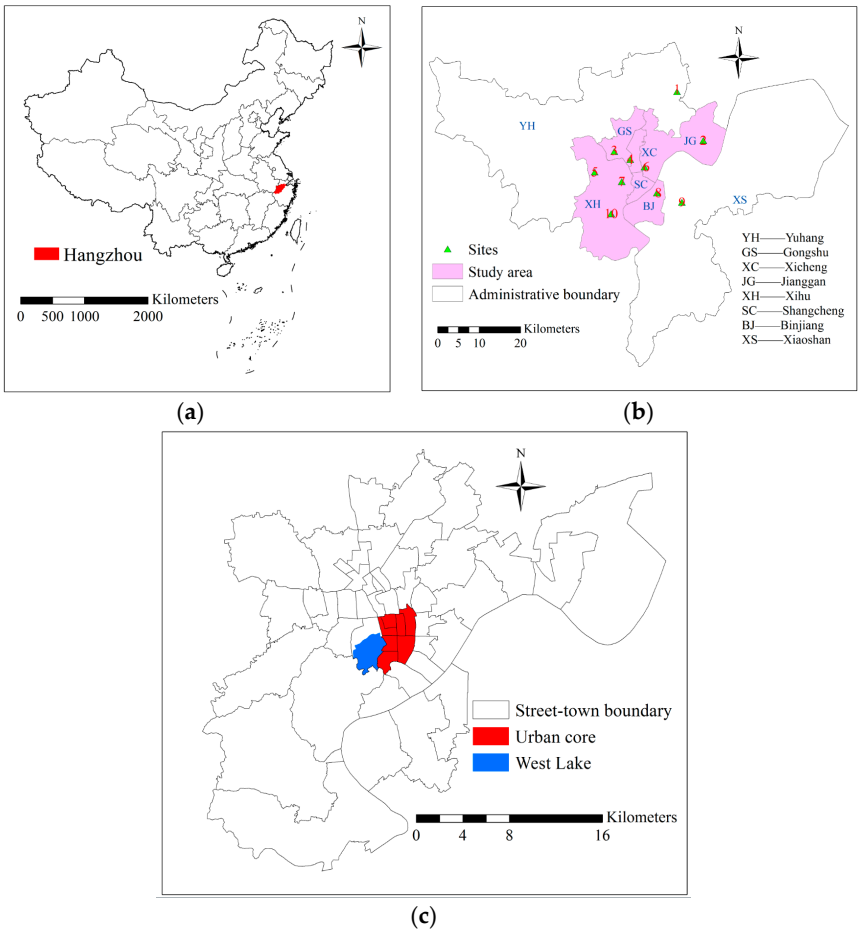

Figure 1. (**a**) Location of Hangzhou in China; (**b**) the spatial distribution of the 10 state-controlled monitoring sites in the eight districts of Hangzhou; (**c**) the street-town boundary, West Lake, and the urban core of the study area.

3. Data Sources and Factors Selection

3.1. Data Sources

The hourly mass concentrations of trace gases (SO_2, NO_2, CO, O_3) and particulate matter ($PM_{2.5}$ and PM_{10}) in the 10 state-controlled monitoring sites of Hangzhou in 2015 are taken from the China National Environmental Monitoring Centre (CNEMC, http://www.cnemc.cn/). Landsat satellite data are recorded for land-use classification and normalized difference vegetation index (NDVI), and land surface temperature (LST) inversion.

3.2. Factor Selection

The concentrations of trace gases and particulate matter are affected by industrial activities, human activities, and traffic emissions. Urban areas are associated with a number of air pollutants and regional pollution problems. Both stationary and mobile sources (vehicles) are major pollution sources in the urban area. Local pollution patterns in cities are mainly related to the different land use and land cover, the layout of transportation network, building and population densities, and the division of functional districts. Pollution levels rise with land-use density, which tends to increase towards a city center [36]. In addition, heat pollution is another type of pollution in urban areas. In this study, population density, road density, built-up density, NDVI, and LST are considered to analyze their relationship with $PM_{2.5}$, PM_{10}, SO_2, NO_2, CO, and O_3.

The urban population has grown in recent years (6.88 million in 2000, 8.70 million in 2010, and 9.00 million in 2015). With rapid urbanization, industrial and commercial activities and the number of vehicles have increased, affecting the atmospheric pollution and poor air quality and impacting the daily life of people living in this area. The gross domestic production was 0.14, 0.60, and 1.01 trillion, respectively, for the years 2000, 2010, and 2015 in Hangzhou City according to the Hangzhou statistical Information Net (http://www.hangzhou.gov.cn/). The number of vehicles was 0.4 million in 2000, 1.8 million in 2010, and 2.6 million in 2015.

In urban areas, due to traffic density and traffic congestion, NO_2 concentrations have increased. The land-use regression models have been used by many for predicting NO_2 [37,38]. Total length of road, road density and traffic density with a specified area are often used as predictor variables in land-use regression models [17,39].

In urban settings, NO_x and volatile organic compounds emissions are typically dominated by anthropogenic sources, primarily from vehicular transport and heavy industry. SO_2 and NO_2 mainly gather in the urban industrial land. In Hangzhou City, the air pollution shows characteristics of SO_2 predominant industry pollution transferred to NO_x predominant living pollution.

The rapid industrialization and urbanization show pronounced changes in land cover, e.g., vegetation is replaced by non-evaporating, non-transpiring surfaces, resulting in a dramatic alteration of the energy balance in the land surface. A higher level of latent heat exchange was found with more vegetated areas, while sensible heat exchange was favored more by sparsely vegetated, urban-impervious areas [40]. The thermal difference, in conjunction with waste heat released from urban houses, industry, and transport, contributed to the development of an urban heat island. Higher urban temperatures generally result in higher ozone levels. In addition, higher urban temperature reflects a growing use of energy, e.g., air conditioning [41].

Vegetation in urban areas is important since it can control environmental conditions and energy exchange by selective reflection and absorption of solar radiations. Also, it is described as an effective factor in air pollution control as it could absorb NO_x and SO_2 pollutants. Here, NDVI is considered one of the most popular indicators for estimating and mapping vegetation coverage.

4. Land-Use Factor Processing

4.1. Population Density

The population density for each street-town unit is defined as the ratio of the census-reported population of the street-town unit to its land area using Equation (1):

$$PD_i = \frac{Pop_i}{Area_i}, \quad (1)$$

where i is the number of street-towns, PD_i refers to the population density of street-town i (persons/km^2), Pop_i represents the population of street-town i, $Area_i$ is the area of street-town i. The sixth national census was conducted in 2010 at the street-town level and published by the administrative districts of Hangzhou. The proportion of the population in each street-town in the year 2010 is based on the sixth national census. In the present study, the population of each street-town in the year 2015 was estimated by multiplying the population in Hangzhou City by the proportion of the population in each street-town. We estimated the population density for the year 2015 for each street-town using Equation (1) (Figure 2). The street-towns with high population density are mainly located in the main urban area and its surrounding areas (Figure 1c).

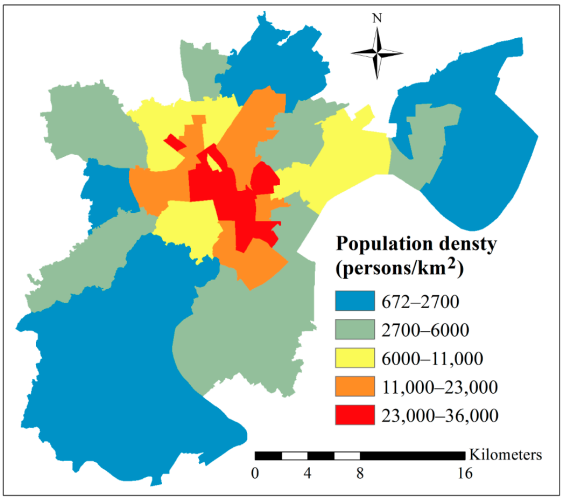

Figure 2. Population density for the street-town unit.

4.2. NDVI and LST

Both NDVI and LST are calculated from the Landsat 8 image. Landsat 8 carries two sensors, the Operational Land Imager (OLI) with nine bands, and the Thermal Infrared Sensor (TIRS) with two bands. Considering the vegetation growth and satellite image quality, we finally chose the Landsat 8 image acquired on 13 October 2015, and the local overpass time of Landsat was 10:31 am. Good vegetation growth and data quality are beneficial for accurate inversion of NDVI and LST, and helpful for extracting the spatial distribution of vegetation and thermal environment information for Hangzhou City and its surroundings.

NDVI, based on spectral reflectance in the near-infrared and visible bands, is widely used for monitoring vegetation cover and ecosystem changes. NDVI is calculated from the following equation:

$$NDVI = \frac{\rho_{nir} - \rho_{red}}{\rho_{nir} + \rho_{red}}, \quad (2)$$

where ρ_{red} and ρ_{nir} are top of atmosphere (TOA) or surface reflectance, respectively, for red and near-infrared wavelengths. The NDVI with the spatial resolution of 30 m is shown in Figure 3a. The average NDVI for the street-town unit is shown in Figure 3b.

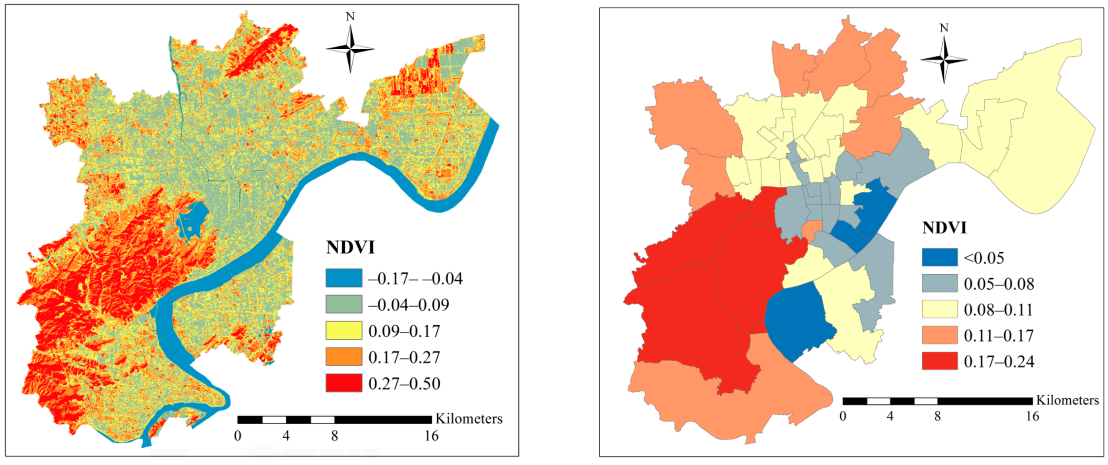

Figure 3. Normalized difference vegetation index (NDVI) retrieved from the Landsat 8 image: (**a**) inversion result with 30 m spatial resolution, and (**b**) average NDVI for street-town unit.

Thermal infrared remote sensing provides a unique approach for retrieving land surface temperature (LST) since the energy detected by the sensor in the spectral region is directly emitted by the land surface. The radiative transfer equation is used to retrieve LST. The radiative transfer equation shows the apparent radiance measured by a sensor:

$$B_i(T_i) = \tau_i(\theta)\left[\varepsilon_i B_i(T_s) + (1-\varepsilon_i)I_i^{\downarrow}\right] + I_i^{\uparrow}, \quad (3)$$

where $B_i(T_i)$ is the radiance received by channel i of the sensor with brightness temperature T_i. $B_i(T_i)$ is composed of three terms: surface emission, atmospheric reflection at the surface, and atmospheric emission. $\tau_i(\theta)$ is the transmittance from the surface to the top of the atmosphere for channel i when the view zenith angle is θ. ε_i represents surface emissivity for channel i. $B_i(T_s)$ refers to the ground radiance at temperature T_s, and T_s is the surface temperature. $I_i^{\downarrow}$ and $I_i^{\uparrow}$ correspond to the downward and upward atmospheric radiances, respectively..

According to Plank's law, $B_i(T_s)$ can be expressed as:

$$B_i(T_s) = 2hc^2 / \left(\lambda_i^5\left(e^{hc/\lambda_i kT_s} - 1\right)\right), \quad (4)$$

where c is the speed of light, h is the Planck constant, k is the Boltzmann constant, and λ_i is the effective band wavelength for band i.

According to Equations (3) and (4), the surface temperature can be calculated from the following equation:

$$T_S = \frac{C_2}{\lambda_i \ln\left(\frac{C_1}{\lambda_i^5\left(B_i(T_i) - I_i^{\uparrow} - \tau_i(1-\varepsilon_i)I_i^{\downarrow}\right)/\tau_i\varepsilon_i} + 1\right)}, \quad (5)$$

where $C_1 = hc^2$, $C_2 = hc/k$ [42,43]. With the thermal radiance measured at sensor level, accompanied by atmospheric parameters, the LST can be calculated using Equation (5). The LST is calculated for each pixel (30 m resolution) using a Landsat image of Hangzhou City (as shown in Figure 4a). The average surface temperature for the street-town unit is shown in Figure 4b.

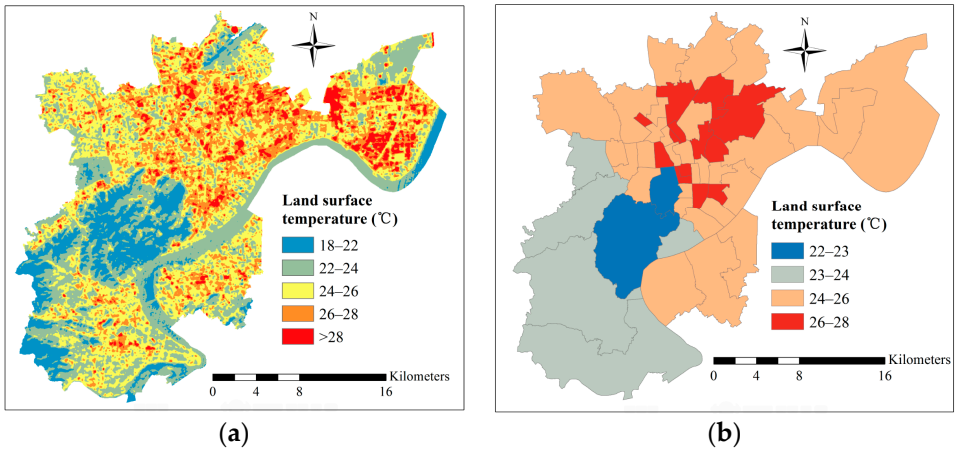

Figure 4. Land surface temperature retrieved from the Landsat 8 image: (**a**) inversion result with 30 m spatial resolution, and (**b**) average surface temperature for street-town unit.

4.3. Urban Build-Up and Road Density

We used visual interpretation and geographic information system (GIS) analysis approach to classify the land use/land cover into seven types: forest land, cropland, water, built-up, road, wetland, and other. The urban built-up area includes residential, industrial, and commercial areas. The built-up areas and roads were extracted to calculate their density for the street-town unit, as follows:

$$CD_i = \frac{Con_i}{Area_i}, \tag{6}$$

$$RD_i = \frac{R_i}{Area_i} \tag{7}$$

where i is the number of street-towns, CD_i refers to the built-up density of street-town i, Con_i represents the built-up area of street-town i, $Area_i$ is the area of street-town i, and RD_i is the road density of street-town i; R_i means the road area of street-town i. The built-up density and road density are shown in Figures 5 and 6.

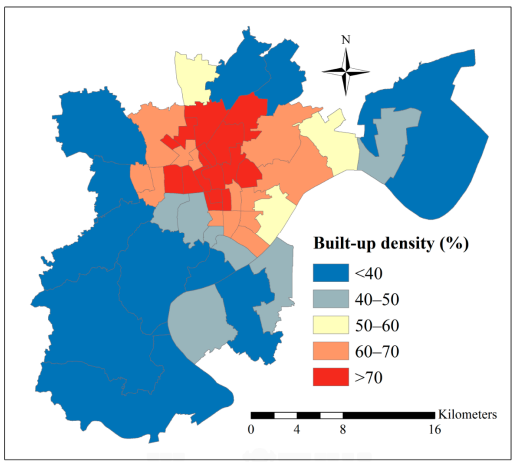

Figure 5. Built-up density for street-town unit.

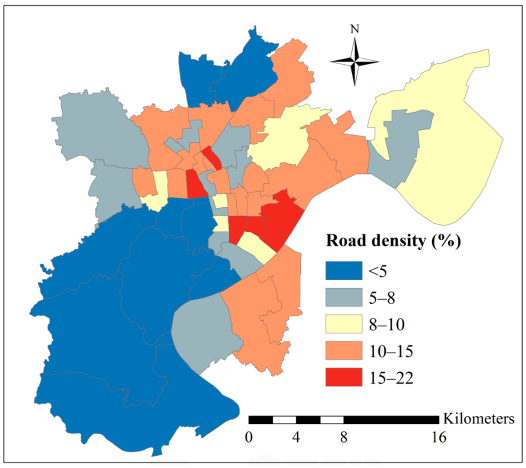

Figure 6. Road density for the street-town unit.

5. Spatiotemporal Distribution of Air Pollution in Hangzhou City

5.1. Temporal Distribution of Air Pollutants

Based on the 10 state-controlled monitoring sites of Hangzhou in the years 2014–2016 (Figure 1b), the monthly and seasonal (spring: March–May, summer: June–August, autumn: September–November, winter: December–February) concentrations and variability of particulate matter ($PM_{2.5}$ and PM_{10}) and trace gases (O_3, SO_2, NO_2, and CO) in Hangzhou are studied. The average concentrations of $PM_{2.5}$, PM_{10}, SO_2, O_3, NO_2, and CO, respectively, are 55.4, 84.7, 50.8, 17.9, 48.8 μg/m^3, and 0.9 mg/m^3 for the years 2014–2016.

The monthly average concentrations of $PM_{2.5}$ and PM_{10} (Figure 7), respectively, show the highest concentrations 87.8 and 127.7 μg/m^3, respectively, in the month of January and December, and the lowest values 36.5 and 59.2 μg/m^3, in the month of July. In addition, the monthly variations of SO_2, NO_2, O_3, and CO for the years 2014–2016 are shown in Figure 8. The concentration of O_3 is highest in the month of May, and lowest in the month of December. Highest concentrations of SO_2 and CO are observed in the month of January.

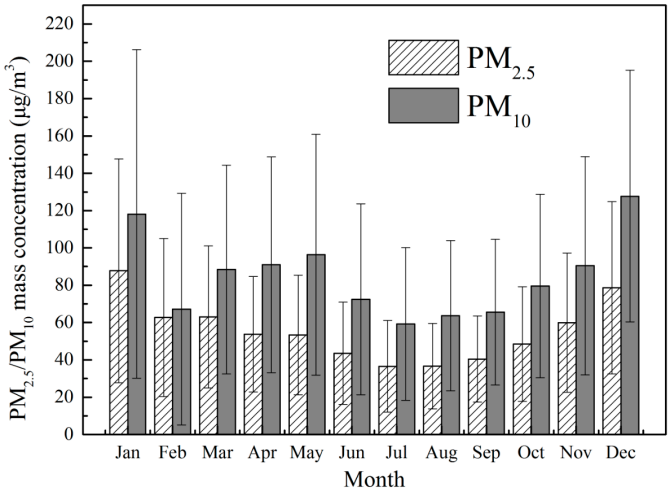

Figure 7. Monthly variations of $PM_{2.5}$, and PM_{10} in Hangzhou City for the years 2014–2016.

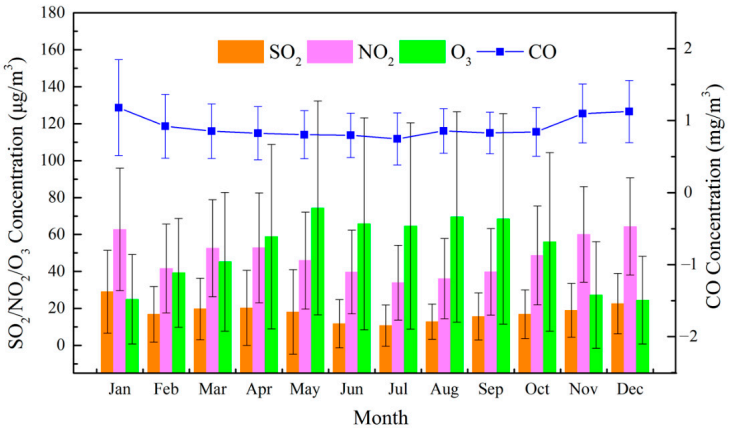

Figure 8. Monthly variations of O_3, SO_2, NO_2, and CO in Hangzhou City for the years 2014–2016.

The seasonal variations of particulate matter and trace gases are shown in Figures 9 and 10. The highest concentration of O_3 is found during summer (66.7 μg/m^3), and the lowest during winter (28.5 μg/m^3). The concentrations of $PM_{2.5}$, PM_{10}, SO_2, NO_2, and CO are observed to be highest during winter, and lowest in summer. During monsoon and typhoon periods, frequent rain cleans the air pollutants [44]. Moreover, the active photochemical reaction consumes precursors of secondary pollutants in the atmosphere, so the concentrations of particulate matter and SO_2, NO_2, and CO are found to be low. However, during winter, the stable weather conditions (e.g., low wind speed) and weak atmospheric diffusion capacity result in high concentrations of particulate matter and trace gases (SO_2, NO_2, and CO). In addition, Hangzhou City has a terrain that descends from southwest to northeast, and the northerly wind prevails during the winter, resulting in poor atmospheric diffusion conditions. Under high temperature and high humidity, SO_2 and NO_x are easier to produce as secondary aerosols. Urban weather features such as the heat island have a great impact on the dispersion of air pollutants. The environmental capacity of Hangzhou City is limited due to the

disadvantageous geographic and meteorological conditions. The major PM sources have changed from coal burning to a mixture of construction sites, coal burning, vehicle exhaust, and secondary particles. Iron/steel manufacturing, secondary aerosols, and local vehicle emissions are suggested as the main sources of $PM_{2.5}$ in Hangzhou City [29,32], with secondary inorganic aerosols playing an important role in haze formation [45].

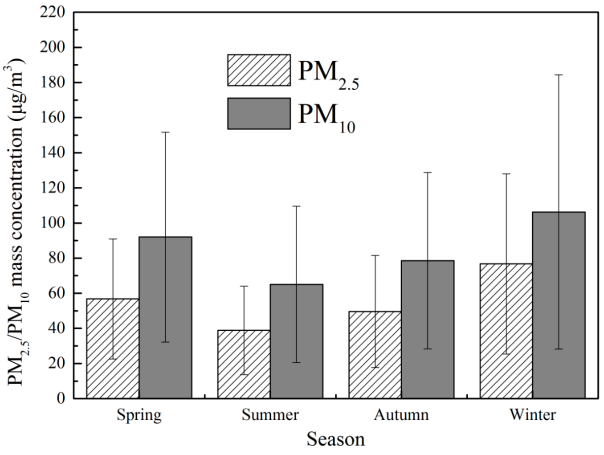

Figure 9. Seasonal variations of $PM_{2.5}$ and PM_{10} in Hangzhou City for 2014–2016.

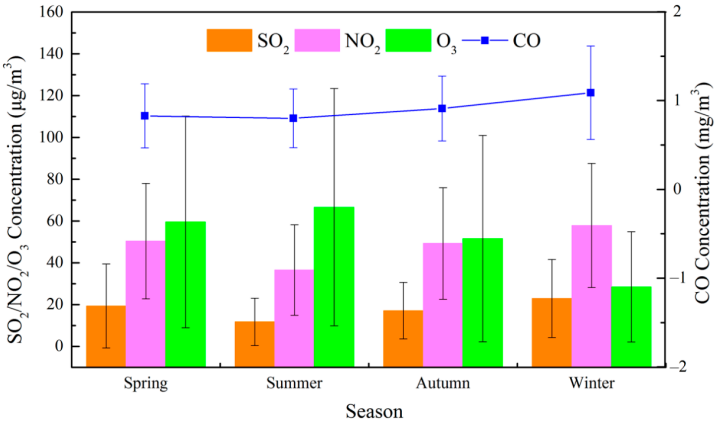

Figure 10. Seasonal variations of SO_2, NO_2, O_3, and CO in Hangzhou City for 2014–2016.

5.2. Spatial Distribution of Air Pollutants

The spatial distribution of seasonal average concentrations of the six air pollutants for years 2014–2016 at the 10 monitoring sites are shown in Figure 11. $PM_{2.5}$ and PM_{10} exhibit similar seasonal variations with the lowest concentrations during summer and the highest during winter for all sites. The lowest $PM_{2.5}$ concentration (31.2 $\mu g/m^3$) is found around site 10 during summer, and the highest $PM_{2.5}$ concentration (86.3 $\mu g/m^3$) is observed around site 3 during winter. The maximum difference of $PM_{2.5}$ (44.5 $\mu g/m^3$) between summer and winter is observed around site 4. The lowest PM_{10} concentration (53.0 $\mu g/m^3$) is found around site 5 during summer, and the highest PM_{10} concentration (121.7 $\mu g/m^3$) is observed around site 1 during winter. The largest value of PM_{10} (60.1 $\mu g/m^3$) difference between summer and winter is observed around site 1. Site 2 has the highest SO_2 concentration (31.1 $\mu g/m^3$) during winter. Meanwhile, the maximum difference of SO_2 (17.5 $\mu g/m^3$) between summer and winter is monitored at site 1. The O_3 concentrations around all sites are lowest during winter, and highest during summer. Site 3 has the highest O_3 concentration (75.8 $\mu g/m^3$) during summer, and site 4 has the lowest O_3 concentration (21.5 $\mu g/m^3$) during winter. The NO_2 concentrations in all sites are lowest during summer, and highest in winter. Site 3 has the

highest NO_2 concentration (65.2 μg/m^3) during winter, and site 10 has the lowest NO_2 concentration (22.3 μg/m^3) during summer. The maximum difference of NO_2 (26.8 μg/m^3) between summer and winter is observed around site 2. The CO concentrations around all sites are highest during winter. The highest CO concentration (1.32 mg/m^3) is observed around site 4 during winter, and the lowest (0.59 mg/m^3) is observed around site 2 during summer. The maximum difference of CO (0.46 mg/m^3) between summer and winter is observed around site 4.

Briefly, during summer, site 10 has the lowest $PM_{2.5}$ concentration (31.2 μg/m^3) and NO_2 concentration (22.3 μg/m^3), site 5 has the lowest PM_{10} concentration (53.0 μg/m^3), site 7 has the lowest SO_2 concentration (6.9 μg/m^3), and site 3 has the highest O_3 concentration (75.8 μg/m^3). During winter, site 3 has the highest $PM_{2.5}$ (86.3 μg/m^3) and NO_2 (65.2 μg/m^3) concentrations, and site 2 has the highest SO_2 (31.1 μg/m^3) concentration. Sites 5, 7, and 10 are located in Xihu district. As the main attraction of Hangzhou, Xihu district is a focus for the protection of scenic spots. In this area, water area is vast, vegetation coverage is high, and tourists visit scenic spots on foot. These factors are conducive to the spread and filtration of particulate matter, making the air quality better. Site 3 is located in Gongshu district (Figure 1b), one of the downtown areas of Hangzhou City. The emission intensity of motor vehicle pollutants shows a decreasing trend from the city center to the city edge. High-emission areas are concentrated in the center and north of the city, mainly because the road network structure is more intensive, and the distribution of commercial and residential areas is relatively concentrated in these areas [46]. Site 2 is located in Jianggang district, which is close to Haining industrial zone. The Haining industrial zone not only blocks the passage of the wind from the north during winter, but also results in a certain source of air pollution in the upwind direction of Jianggang district. In addition, site 1 has the highest variations of SO_2 (17.5 μg/m^3) and PM_{10} (60.1 μg/m^3) between summer and winter. Site 4 has the highest variations of $PM_{2.5}$ (44.5 μg/m^3) and CO (0.46 mg/m^3) between summer and winter. Site 2 has the highest variations of NO_2 (26.8 μg/m^3) and O_3 (48.1 μg/m^3) between summer and winter.

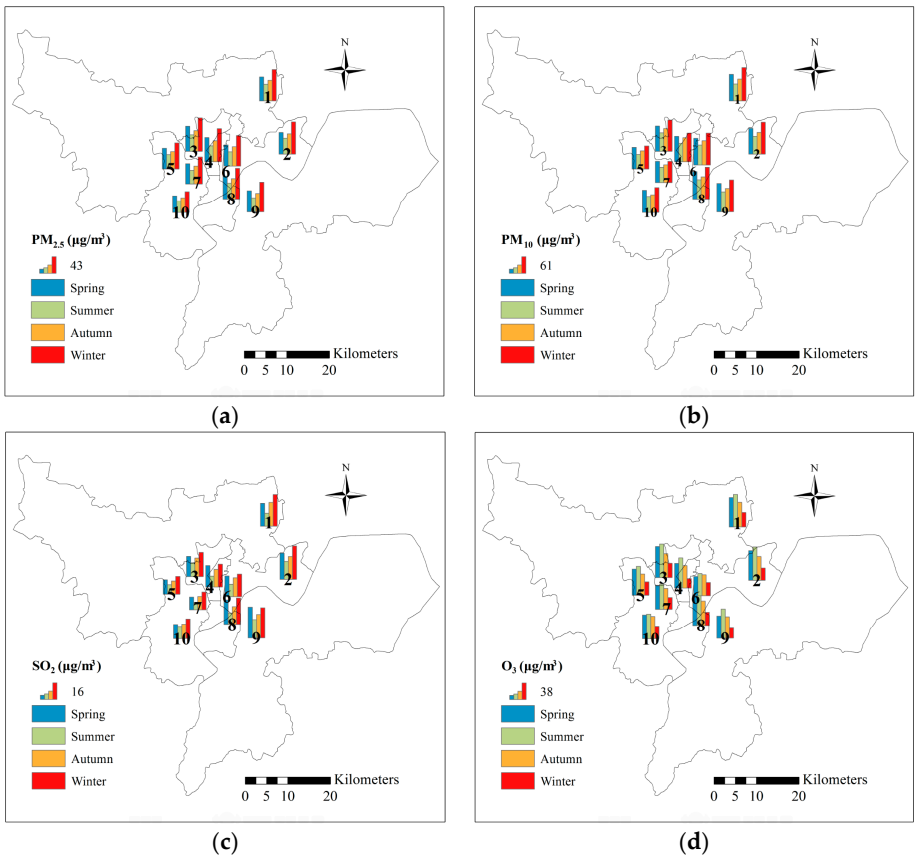

Figure 11. *Cont.*

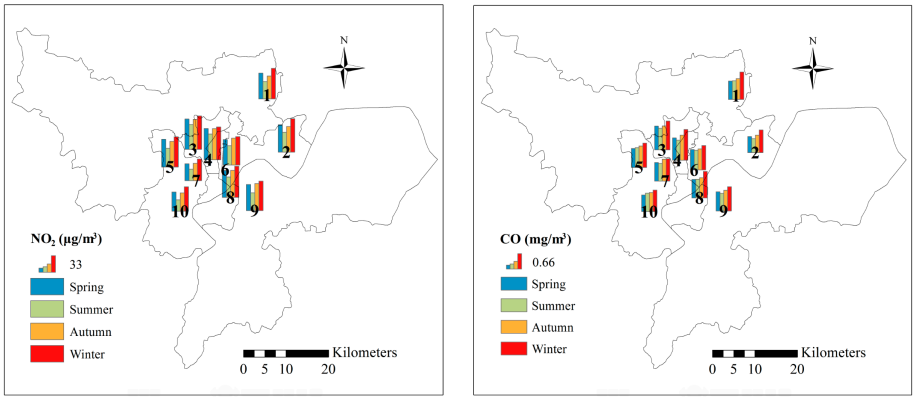

(**e**) (**f**)

Figure 11. Spatial distribution of seasonal average concentrations of particulate matter and trace gases in Hangzhou City for 2014–2016: (**a**) $PM_{2.5}$ (μg/m^3); (**b**) PM_{10} (μg/m^3); (**c**) SO_2 (μg/m^3); (**d**) O_3 (μg/m^3); (**e**) NO_2 (μg/m^3); (**f**) CO (mg/m^3).

5.3. Spatial Interpolation of Air Pollutants

For the quantitative relationship between air pollution and land use, we interpolated the annual average concentrations of particulate matter and trace gases from 10 monitoring sites in Hangzhou City and surroundings by an ordinary kriging method. We adopted kriging interpolation because this stochastic method produces the best linear unbiased estimation of the pollution level [47]. The kriging interpolations of annual average concentrations of $PM_{2.5}$, PM_{10}, SO_2, O_3, NO_2, and CO for 2015 are shown in Figure 12. Both $PM_{2.5}$ and PM_{10} show high concentrations in the middle region compared with the western parts of the Hangzhou region. The concentration of SO_2 increases from west to east. A low concentration of O_3 is observed in the central region, and a high value is observed in north-central and south-central regions. The annual CO level decreases from north to south. The average concentrations of each air pollutants for the street-town unit are quantitatively calculated for the quantitative analysis.

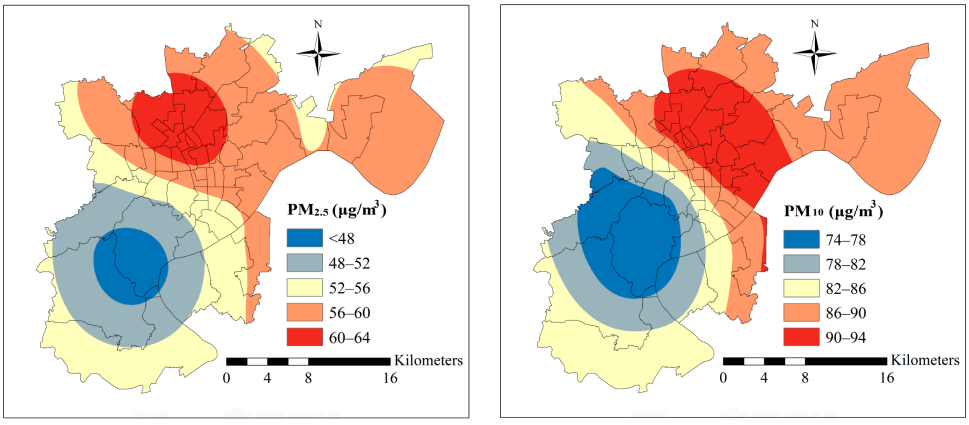

(**a**) (**b**)

Figure 12. *Cont.*

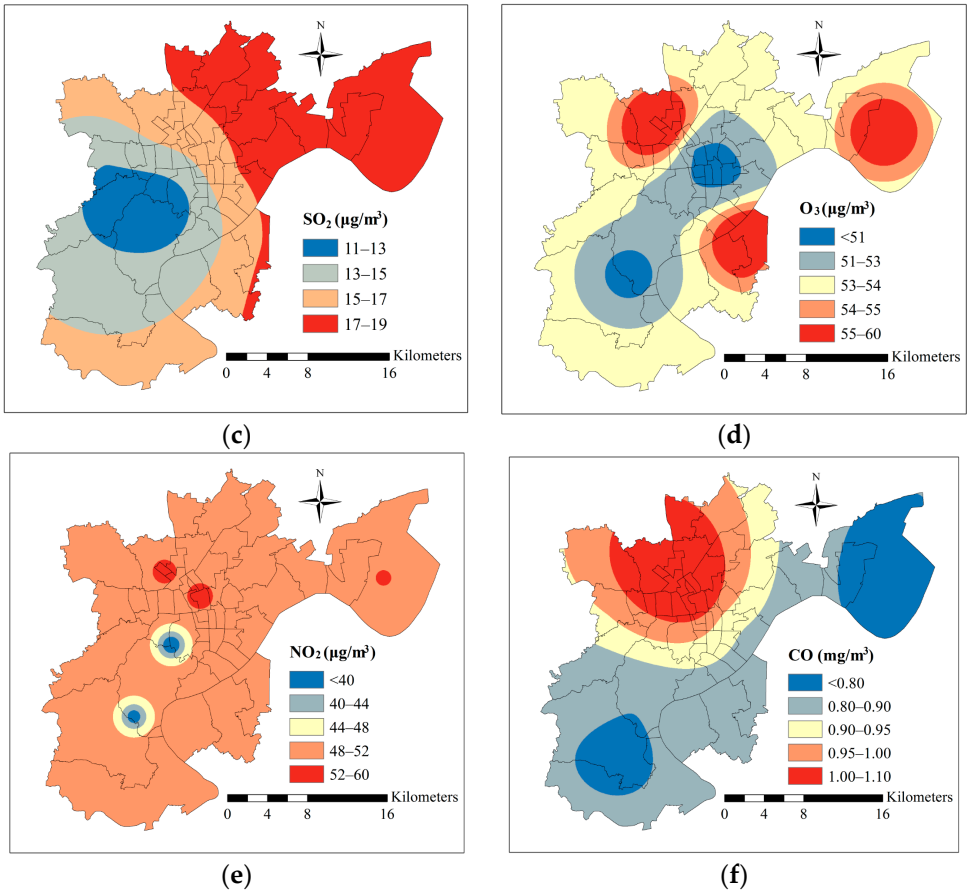

Figure 12. Spatial distribution of annual average concentrations of particulate matter and trace gases in Hangzhou City for 2015: (**a**) $PM_{2.5}$ (μg/m^3); (**b**) PM_{10} (μg/m^3); (**c**) SO_2 (μg/m^3); (**d**) O_3 (μg/m^3); (**e**) NO_2 (μg/m^3); (**f**) CO (mg/m^3).

6. Results and Discussion

The relationship between air pollutants and land use was analyzed at the street-town unit level in Hangzhou City for 2015. There are 49 street-towns in the Hangzhou area (Figure 1c), and 49 groups of data used in the correlation analysis. The Spearman's rank correlation with SPSS software version 16.0 (SPSS Inc., Chicago, IL, USA) is used in the present study. Spearman's rank correlation is a non-parametric measure of statistical dependence between two variables. The exact sample distribution is obtained without requiring knowledge of the probability distribution of variables. The correlation analysis between land-use change and air pollutants is shown in Table 2. A strong correlation is found between the concentrations of air pollutants and land use. From the perspective of land use, road density shows a pronounced positive correlation (R = 0.39, 0.45, 0.32, 0.48) with $PM_{2.5}$, PM_{10}, SO_2, and NO_2, and weak positive correlation (R = 0.02, 0.2) with O_3 and CO. The built-up density shows a strong positive correlation (R = 0.78, 0.67, 0.63, 0.69) with $PM_{2.5}$, PM_{10}, NO_2, and CO pollution, as well as population density (R = 0.55, 0.42, 0.56, 0.57). LST shows a strong positive correlation (R = 0.67, 0.69, 0.49, 0.46, 0.47) with $PM_{2.5}$, PM_{10}, SO_2, NO_2, and CO, while NDVI shows a strong negative correlation (R = −0.29, −0.29) with PM_{10} and NO_2, and weak negative correlation (R = −0.19, −0.07, −0.08) with $PM_{2.5}$, SO_2, and CO. The areas with low NDVI, high built-up density, road density, and LST are consistent with high concentrations of $PM_{2.5}$, PM_{10}, SO_2, NO_2, CO pollution.

Table 2. Spearman's rank correlation between air pollutants and land use.

	Air Pollutants						Land Use				
	$PM_{2.5}$	PM_{10}	SO_2	O_3	NO_2	CO	RD	CD	NDVI	LST	PD
$PM_{2.5}$	—										
PM_{10}	0.780 **	—									
SO_2	0.437 **	0.750 **	—								
O_3	0.118	−0.124	0.172	—							
NO_2	0.730 **	0.560 **	0.223	0.098	—						
CO	0.861 **	0.465 **	−0.006	0.087	0.579 **	—					
RD	0.394 **	0.450 **	0.318 *	0.024	0.475 **	0.204	—				
BD	0.784 **	0.667 **	0.191	−0.246	0.628 **	0.688 **	0.447 **	—			
NDVI	−0.187	−0.294 *	−0.068	0.263	−0.294 *	−0.084	−0.455 **	−0.514 **	—		
LST	0.670 **	0.685 **	0.487 **	−0.113	0.461 **	0.471 **	0.509 **	0.772 **	−0.312 *	—	
PD	0.551 **	0.415 **	−0.082	−0.333 *	0.562 **	0.566 **	0.531 **	0.816 **	−0.606 **	0.615 **	—

RD-Road density, BD-Built-up density, LST-Land surface temperature, PD-Population density; ** Correlation is significant at the 0.01 level (2-tailed); * Correlation is significant at the 0.05 level (2-tailed).

For particle matter, $PM_{2.5}$ shows pronounced positive correlation with land-use effects except NDVI, especially with built-up density and LST with the correlation coefficient higher than 0.6. For PM_{10}, there is a strong positive correlation (R = 0.67, 0.69) with built-up density and LST, but a negative correlation (R = −0.29) with NDVI. Vegetation could deposit particulate matter, while built-up areas could produce particulate matter. A similar relationship between particulate pollution and land use is observed in representative cities of China. Strong correlations between particulate pollution and urban land, woodland, and grassland are found [48]. The effects of landscape pattern on $PM_{2.5}$ concentration by means of correlation analysis are also explored in Beijing. Vegetation can significantly reduce $PM_{2.5}$ concentration, while construction land increases the concentration [49]. For trace gases, O_3 shows a weak correlation with land use. SO_2 shows a strong positive correlation (R = 0.32, 0.49) with road density and LST. A street-town unit with high road density could reflect the convenient transportation of this area, and is considered to have a higher probability of being used for industrial and mining warehouses, and as a business center. The positive correlation between SO_2 and road density and LST means the denser the roads, the more emissions from industry and traffic exhaust, causing an increase in SO_2 concentration. In addition, the pronounced correlation between road density and LST (R = 0.51) is associated with traffic road materials and exhaust heat of vehicles; LST over roads is much higher than over other land cover, as found earlier [50]. NO_2 shows a strong positive correlation with road density, built-up density, LST, and population density, with a correlation coefficient higher than 0.46, while there is a strong negative correlation (R = −0.29) with NDVI. NO_2 is the most affected by land use among the trace gases. NO_2 is a good indicator of traffic-related pollution. In earlier studies of NO_2 prediction using the LUR model, NO_2 showed a positive correlation with road length, built-up area, and population, but a negative correlation with agricultural land area and tree canopy [20,51]. CO shows a strong positive correlation (R = 0.69, 0.47, 0.57) with built-up density, LST, and population density. The results show that the urban concentration of CO is strongly influenced by production activities in the built-up area and emissions from residents' stoves. A similar relationship of air pollution (SO_2, NO_x, and dust) with urban land use and the urban thermal landscape is observed in Guangzhou City, China. Results show that the spatial patterns of air pollutants are positively correlated with urban built-up density and satellite-derived land surface temperature [41].

In the present study, we have used the Landsat 8 acquired in October to retrieve NDVI and LST, representing the spatial distribution of vegetation and thermal environment information in Hangzhou. With the introduction of satellite data in different months, the spatial distribution could be more detailed and accurate. There is no doubt that particulate matter and trace gases are controlled by many factors besides the variables in the present study. With the rapid development of data sharing around the world, there would be more potential variables included in the correlation analysis.

7. Conclusions

We have shown the spatial and monthly/seasonal variability of air pollutants (particulate matter and trace gases) Hangzhou City for the years 2014–2016. The annual average concentrations of $PM_{2.5}$, PM_{10}, SO_2, O_3, NO_2, and CO are 55.4, 84.7, 50.8, 17.9, 48.8 $\mu g/m^3$, and 0.9 mg/m^3, respectively. $PM_{2.5}$ and PM_{10} show strong inter-monthly dynamics, with the lowest values in the month of July. Meanwhile, trace gases (SO_2 and CO) show the highest values in the month of January, while O_3 shows the highest value in the month of May. Due to the disadvantageous geographic and meteorological conditions, air pollutants are difficult to disperse. Coal burning, construction, vehicle exhaust, and secondary particles are the main sources of air pollutants. From the seasonal variation, $PM_{2.5}$, PM_{10}, SO_2, NO_2, and CO concentrations are observed to be highest during winter due to the stable weather conditions and northerly winds, and lowest in summer due to the clean marine air during the monsoon period, and the concentration of O_3 is highest during summer and lowest in winter. From the spatial distribution of air pollutants in Hangzhou City, low concentrations of $PM_{2.5}$ PM_{10}, and SO_2 are observed during summer in Xihu district. Due to high vehicular emissions concentrated in the center and north of the city, high $PM_{2.5}$, NO_2, and CO are observed during winter in Gongshu and Xiacheng districts. In addition, we have analyzed the correlation between air pollutants and land-use change at the street-town level. From the perspective of land use, through the correlation analysis, it is found that high built-up density, road density, LST, and low NDVI are consistent with increasing concentrations of $PM_{2.5}$, PM_{10}, SO_2, NO_2, CO. For particulate matter, both $PM_{2.5}$ and PM_{10} have a strong positive correlation with built-up density and LST. Among trace gases, O_3 shows weak correlation with land use, and NO_2 is the most sensitive element affected by land use among the trace gases. SO_2 shows pronounced positive correlation with road density and LST. CO shows a positive correlation with built-up density, LST, and population density. The street-towns are the smallest geographic unit at which census data are released. At the street-town scale, the social and environmental data are more detailed and accurate. Detailed information on the relationship between air pollutants and land use at the street-town level in the Hangzhou area will be very useful to urban and environmental planners in formulating urban design and landscape policies for ecological improvement and sustainable economic growth.

Acknowledgments: The present work is supported by the Scientific Research Project of the Education Department of Zhejiang Province (Grant No. Y201636214), Fundamental Research Funds for the Central Universities, and the National Social Science Foundation of China (Grant No. 14ZDA039). The authors are grateful to the China National Environmental Monitoring Centre for making trace gases and particulate matter data for 2014–2016 available for Hangzhou, China. Our thanks to the Landsat team for providing Landsat data. The authors are grateful to the two anonymous referees, who were very useful in improving an earlier version of the manuscript.

Author Contributions: Sheng Zheng wrote the paper, Xueyuan Zhou analyzed the data, Ramesh P. Singh designed the study, Yuzhe Wu collected the data, Yanmei Ye discussed the results, Cifang Wu contributed the central idea.

Conflicts of Interest: The authors declare no conflict of interest.

References

1. Crutzen, P.J. Geology of mankind. *Nature* **2002**, *415*, 23. [CrossRef] [PubMed]
2. Lelieveld, J.; Barlas, C.; Giannadaki, D.; Pozzer, A. Model calculated global, regional and megacity premature mortality due to air pollution. *Atmos. Chem. Phys.* **2013**, *13*, 7023–7037. [CrossRef]
3. Lim, S.S.; Vos, T.; Flaxman, A.D.; Danaei, G.; Shibuya, K.; Adair-Rohani, H.; AlMazroa, M.A.; Amann, M.; Anderson, H.R.; Andrews, K.G.; et al. A comparative risk assessment of burden of disease and injury attributable to 67 risk factors and risk factor clusters in 21 regions, 1990–2010: A systematic analysis for the global burden of disease study 2010. *Lancet* **2013**, *380*, 2224–2260. [CrossRef]
4. Contini, D.; Cesari, D.; Genga, A.; Siciliano, M.; Ielpo, P.; Guascito, M.; Conte, M. Source apportionment of size-segregated atmospheric particles based on the major water-soluble components in Lecce (Italy). *Sci. Total Environ.* **2014**, *472*, 248–261. [CrossRef] [PubMed]

5. Tan, J.; Duan, J.; Zhen, N.; He, K.; Hao, J. Chemical characteristics and source of size-fractionated atmospheric particle in haze episode in Beijing. *Atmos. Res.* **2016**, *167*, 24–33. [CrossRef]
6. Xing, R.; Hanaoka, T.; Kanamori, Y.; Dai, H.; Masui, T. An impact assessment of sustainable technologies for the Chinese urban residential sector at provincial level. *Environ. Res. Lett.* **2015**, *10*, 065001. [CrossRef]
7. Yu, S.; Zhang, Q.; Yan, R.; Wang, S.; Li, P.; Chen, B.; Liu, W.; Zhang, X. Origin of air pollution during a weekly heavy haze episode in Hangzhou, China. *Environ. Chem. Lett.* **2014**, *12*, 543–550. [CrossRef]
8. Zhao, J.; Zhang, F.; Xu, Y.; Chen, J. Characterization of water-soluble inorganic ions in size-segregated aerosols in coastal city, Xiamen. *Atmos. Res.* **2011**, *99*, 546–562. [CrossRef]
9. Heald, C.L.; Spracklen, D.V. Land use change impacts on air quality and climate. *Chem. Rev.* **2015**, *115*, 4476–4496. [CrossRef] [PubMed]
10. Crutzen, P.J.; Andreae, M.O. Biomass burning in the tropics: Impact on atmospheric chemistry and biogeochemical cycles. *Science* **1990**, *250*, 1669–1678. [CrossRef] [PubMed]
11. Houghton, R.; Hobbie, J.; Melillo, J.M.; Moore, B.; Peterson, B.; Shaver, G.; Woodwell, G. Changes in the carbon content of terrestrial biota and soils between 1860 and 1980: A net release of CO_2 to the atmosphere. *Ecol. Monogr.* **1983**, *53*, 235–262. [CrossRef]
12. Cicerone, R.J.; Oremland, R.S. Biogeochemical aspects of atmospheric methane. *Glob. Biogeochem. Cycles* **1988**, *2*, 299–327. [CrossRef]
13. MacFarling Meure, C.; Etheridge, D.; Trudinger, C.; Steele, P.; Langenfelds, R.; Van Ommen, T.; Smith, A.; Elkins, J. Law dome CO_2, CH_4 and N_2O ice core records extended to 2000 years BP. *Geophys. Res. Lett.* **2006**, *33*, L14810. [CrossRef]
14. Lerner, J.; Matthews, E.; Fung, I. Methane emission from animals: A global high-resolution data base. *Glob. Biogeochem. Cycles* **1988**, *2*, 139–156. [CrossRef]
15. Taha, H. Modeling impacts of increased urban vegetation on ozone air quality in the south coast air basin. *Atmos. Environ.* **1996**, *30*, 3423–3430. [CrossRef]
16. Peng, W.; Zhou, J.; Luo, H.; Yang, C.; Zhao, J. Relationship between land use change and its urban air environmental impacts. *Res. Soil Water Conserv.* **2010**, *17*, 87–91. (In Chinese)
17. Hankey, S.; Marshall, J.D. Land use regression models of on-road particulate air pollution (particle number, black carbon, $PM_{2.5}$, particle size) using mobile monitoring. *Environ. Sci. Technol.* **2015**, *49*, 9194–9202. [CrossRef] [PubMed]
18. Knibbs, L.D.; Hewson, M.G.; Bechle, M.J.; Marshall, J.D.; Barnett, A.G. A national satellite-based land-use regression model for air pollution exposure assessment in Australia. *Environ. Res.* **2014**, *135*, 204–211. [CrossRef] [PubMed]
19. Knibbs, L.D.; Coorey, C.P.; Bechle, M.J.; Cowie, C.T.; Dirgawati, M.; Heyworth, J.S.; Marks, G.B.; Marshall, J.D.; Morawska, L.; Pereira, G.; et al. Independent validation of national satellite-based land-use regression models for nitrogen dioxide using passive samplers. *Environ. Sci. Technol.* **2016**, *50*, 12331–12338. [CrossRef] [PubMed]
20. Novotny, E.V.; Bechle, M.J.; Millet, D.B.; Marshall, J.D. National satellite-based land-use regression: NO_2 in the United States. *Environ. Sci. Technol.* **2011**, *45*, 4407–4414. [CrossRef] [PubMed]
21. Vienneau, D.; de Hoogh, K.; Bechle, M.J.; Beelen, R.; van Donkelaar, A.; Martin, R.V.; Millet, D.B.; Hoek, G.; Marshall, J.D. Western European land use regression incorporating satellite- and ground-based measurements of NO_2 and PM_{10}. *Environ. Sci. Technol.* **2013**, *47*, 13555–13564. [CrossRef] [PubMed]
22. Yeganeh, B.; Hewson, M.G.; Clifford, S.; Knibbs, L.D.; Morawska, L. A satellite-based model for estimating $PM_{2.5}$ concentration in a sparsely populated environment using soft computing techniques. *Environ. Model. Softw.* **2017**, *88*, 84–92. [CrossRef]
23. Clark, L.P.; Millet, D.B.; Marshall, J.D. Air quality and urban form in us urban areas: Evidence from regulatory monitors. *Environ. Sci. Technol.* **2011**, *45*, 7028–7035. [CrossRef] [PubMed]
24. Bechle, M.J.; Millet, D.B.; Marshall, J.D. Effects of income and urban form on urban NO_2: Global evidence from satellites. *Environ. Sci. Technol.* **2011**, *45*, 4914–4919. [CrossRef] [PubMed]
25. Liao, J.; Wang, T.; Jiang, Z.; Zhuang, B.; Xie, M.; Yin, C.; Wang, X.; Zhu, J.; Fu, Y.; Zhang, Y. WRF/Chem modeling of the impacts of urban expansion on regional climate and air pollutants in Yangtze River Delta, China. *Atmos. Environ.* **2015**, *106*, 204–214. [CrossRef]

26. Cheng, Z.; Wang, S.; Jiang, J.; Fu, Q.; Chen, C.; Xu, B.; Yu, J.; Fu, X.; Hao, J. Long-term trend of haze pollution and impact of particulate matter in the Yangtze River Delta, China. *Environ. Pollut.* **2013**, *182*, 101–110. [CrossRef] [PubMed]
27. Cheng, Z.; Wang, S.; Fu, X.; Watson, J.; Jiang, J.; Fu, Q.; Chen, C.; Xu, B.; Yu, J.; Chow, J. Impact of biomass burning on haze pollution in the Yangtze River Delta, china: A case study in summer 2011. *Atmos. Chem. Phys.* **2014**, *14*, 4573–4585. [CrossRef]
28. Zhang, Q.Y.; Li, X.X.; Tian, W.L.; Fu, A.Y.; Du, W.F.; Wang, C. Scenarios for vehicular air pollutant emissions abatement: A case study in Hangzhou, China. *J. Zhejiang Univ. Sci.* **2014**, *15*, 753–760. [CrossRef]
29. Liu, G.; Li, J.; Wu, D.; Xu, H. Chemical composition and source apportionment of the ambient $PM_{2.5}$ in Hangzhou, China. *Particuology* **2015**, *18*, 135–143. [CrossRef]
30. Liu, H.; Ma, W.; Qian, J.; Cai, J.; Ye, X.; Li, J.; Wang, X. Effect of urbanization on the urban meteorology and air pollution in Hangzhou. *J. Meteorol. Res.* **2015**, *29*, 950–965. [CrossRef]
31. Peng, Z.R.; Wang, D.; Wang, Z.; Gao, Y.; Lu, S. A study of vertical distribution patterns of $PM_{2.5}$ concentrations based on ambient monitoring with unmanned aerial vehicles: A case in Hangzhou, China. *Atmos. Environ.* **2015**, *123*, 357–369. [CrossRef]
32. Wu, J.; Xu, C.; Wang, Q.; Cheng, W. Potential sources and formations of the $PM_{2.5}$ pollution in urban Hangzhou. *Atmosphere* **2016**, *7*, 100. [CrossRef]
33. Hangzhou Statistics Bureau. *Hangzhou Statistical Yearbook 2014*; China Statistics Press: Beijing, China, 2014. (In Chinese)
34. Wang, J.; Zhang, J.S.; Liu, Z.J.; Wu, J.H.; Zhang, Y.F.; Han, S.Q.; Zheng, X.J.; Zhou, L.D.; Feng, Y.C.; Zhu, T. Characterization of chemical compositions in size-segregated atmospheric particles during severe haze episodes in three mega-cities of China. *Atmos. Res.* **2017**, *187*, 138–146. [CrossRef]
35. Wang, F.; Zhou, Y. Modelling urban population densities in Beijing 1982–1990: Suburbanisation and its causes. *Urban Stud.* **1999**, *36*, 271–287. [CrossRef]
36. Marsh, W.M.; Grossa, J. *Environmental Geography: SCIENCE, Land Use, and Earth Systems*, 3rd ed.; Wiley: New York, NY, USA, 2005.
37. Hoek, G.; Beelen, R.; de Hoogh, K.; Vienneau, D.; Gulliver, J.; Fischer, P.; Briggs, D. A review of land-use regression models to assess spatial variation of outdoor air pollution. *Atmos. Environ.* **2008**, *42*, 7561–7578. [CrossRef]
38. Marshall, J.D.; Nethery, E.; Brauer, M. Within-urban variability in ambient air pollution: Comparison of estimation methods. *Atmos. Environ.* **2008**, *42*, 1359–1369. [CrossRef]
39. Rose, N.; Cowie, C.; Gillett, R.; Marks, G.B. Weighted road density: A simple way of assigning traffic-related air pollution exposure. *Atmos. Environ.* **2009**, *43*, 5009–5014. [CrossRef]
40. Oke, T.R. The energetic basis of the urban heat island. *Q. J. R. Meteor. Soc.* **1982**, *108*, 1–24. [CrossRef]
41. Weng, Q.; Yang, S. Urban air pollution patterns, land use, and thermal landscape: An examination of the linkage using GIS. *Environ. Monit. Assess.* **2006**, *117*, 463–489. [CrossRef] [PubMed]
42. Ottlé, C.; Stoll, M. Effect of atmospheric absorption and surface emissivity on the determination of land surface temperature from infrared satellite data. *Int. J. Remote Sens.* **1993**, *14*, 2025–2037. [CrossRef]
43. Yu, X.; Guo, X.; Wu, Z. Land surface temperature retrieval from Landsat 8 TIRS-comparison between radiative transfer equation-based method, split window algorithm and single channel method. *Remote Sens. Basel* **2014**, *6*, 9829. [CrossRef]
44. Wang, J.; Hu, Z.; Chen, Y.; Chen, Z.; Xu, S. Contamination characteristics and possible sources of PM_{10} and $PM_{2.5}$ in different functional areas of Shanghai, China. *Atmos. Environ.* **2013**, *68*, 221–229. [CrossRef]
45. Jansen, R.C.; Shi, Y.; Chen, J.; Hu, Y.; Xu, C.; Hong, S.; Li, J.; Zhang, M. Using hourly measurements to explore the role of secondary inorganic aerosol in $PM_{2.5}$ during haze and fog in Hangzhou, China. *Adv. Atmos. Sci.* **2014**, *31*, 1427–1434. [CrossRef]
46. Wang, X.W.; Tian, W.L.; Zhang, Q.Y. Development of motor vehicles emission inventory in Hangzhou. *China Environ. Sci.* **2012**, *32*, 1368–1374. (In Chinese)
47. Burrough, P.A.; Mcdonnell, R.A.; Lloyd, C.D. *Principles of Geographical Information Systems*; Oxford University Press: Oxford, UK, 1998.
48. Sun, L.; Wei, J.; Duan, D.; Guo, Y.; Yang, D.; Jia, C.; Mi, X. Impact of land-use and land-cover change on urban air quality in representative cities of china. *J. Atmos. Sol. Terr. Phys.* **2016**, *142*, 43–54. [CrossRef]

49. Wu, J.; Xie, W.; Li, W.; Li, J. Effects of urban landscape pattern on $PM_{2.5}$ pollution—A Beijing case study. *PLoS ONE* **2015**, *10*. [CrossRef] [PubMed]
50. Yuan, F.; Bauer, M.E. Comparison of impervious surface area and normalized difference vegetation index as indicators of surface urban heat island effects in Landsat imagery. *Remote Sens. Environ.* **2007**, *106*, 375–386. [CrossRef]
51. Meng, X.; Chen, L.; Cai, J.; Zou, B.; Wu, C.F.; Fu, Q.; Zhang, Y.; Liu, Y.; Kan, H. A land use regression model for estimating the NO_2 concentration in Shanghai, China. *Environ. Res.* **2015**, *137*, 308–315. [CrossRef] [PubMed]